Mechanics Research Communications xxx (2016) xxx–xxx

Contents lists available at ScienceDirect

Mechanics Research Communications

journal homepage: www.elsevier.com/locate/mechrescom

Fluid flow in fractured and fracturing porous media: A unified view

René de Borst*

University of Sheffield, Department of Civil and Structural Engineering, Mappin Street, Sir Frederick Mappin Building, Sheffield S1 3JD, UK

ARTICLE INFO

Article history:
Received 2 March 2016
Received in revised form 10 May 2016
Accepted 16 May 2016
Available online xxx

Keywords:
Fracture
Porous media
Interface elements
Extended finite element method
Isogeometric analysis

ABSTRACT

Fluid flow in fractures that pre-exist or propagate in a porous medium can have a major influence on the deformation and flow characteristics. With the aim of carrying out large-scale calculations at reasonable computing costs, a sub-grid scale model has been developed. While this model was originally embedded in extended finite element methods, thereby exploiting some special properties of the enrichment functions, we will herein show that, using proper micro–macro relations, in particular for the mass balance, sub-grid scale models can be coupled to a range of discretisation methods at the macroscopic scale, from standard interface elements to isogeometric finite element analysis.

1. Introduction

Stationary or propagating cracks in (partially) saturated porous media occur frequently in a number of important applications. The existence and propagation of such cracks can be undesirable, such as in human tissues, or for the storage of waste in rocks or salt domes, but at other times cracking can be a pivotal element in an industrial process, for example hydraulic fracturing in the oil and gas industry. Another important application is the rupture of geological faults, where the change in geometry of a fault can drastically affect local fluid flow as the faults can act as channels in which the fluid can flow freely.

The first approaches to the propagation of fluid-saturated cracks were of an analytical nature [1–4]. For idealised geometries and considering the surrounding medium as linear elastic, homogeneous and impervious, an ad hoc leak-off term was introduced to account for the fluid loss into the surrounding medium [5]. Linear elastic fracture mechanics was used to derive a crack propagation criterion. Invoking scaling laws, Detournay [6] has put these works on a solid basis, and has identified that, depending on, *inter alia*, the values for the fracture toughness and the fluid viscosity, different propagation regimes can be distinguished.

A model to capture fluid flow in a *porous* medium intersected by multiple cracks was proposed by Barenblatt et al. [7]. Building on the latter approach, in which the porous medium was assumed to be rigid, Aifantis and co-workers generalised this idea and developed the double porosity model [8–10], wherein Biot's theory for deformable porous media [11] was exploited. The double porosity model describes the effects of cracks on fluid flow and vice versa in a homogenised sense, but the *local* interaction of a crack and the fluid flow is not captured.

This is different when the crack is accounted for explicitly. The oldest, and still very powerful method is to adapt the geometry of the body via remeshing. Originally, this was done using linear elastic fracture mechanics, and for applications to fracture propagation of fluid-pressurised cracks reference is made to [12,13]. More recently, fluid-saturated cohesive cracks have also been modelled [14–17].

A sub-grid scale model for the transport and storage of fluids in pre-existing or propagating cracks has been developed by De Borst and co-workers [18,19], see also [20,21], Fig. 1. Starting from the local mass and momentum balances for the fluid in the crack and exploiting the observation that the width of the crack is small compared to the other dimensions of the crack, the sub-grid scale model has been coupled to the mass and momentum balances at global level. In this fashion, the possibility has been opened to analyse deformation and fluid flow in large formations that contain multiple cracks.

Originally tightly coupled to the extended finite element method, we will herein show that this sub-grid scale model can be embedded in other discretisation frameworks as well, including, for instance, interface elements enhanced with pressure degrees-of-freedom [22–24]. It is furthermore noted that the extended finite element method has also been used to describe fracture propagation in porous media without a sub-grid scale model [25–28], also in combination with level sets to pin-point the crack front [29].

* Tel.: +44 1142225796.
E-mail address: r.deborst@sheffield.ac.uk

http://dx.doi.org/10.1016/j.mechrescom.2016.05.004

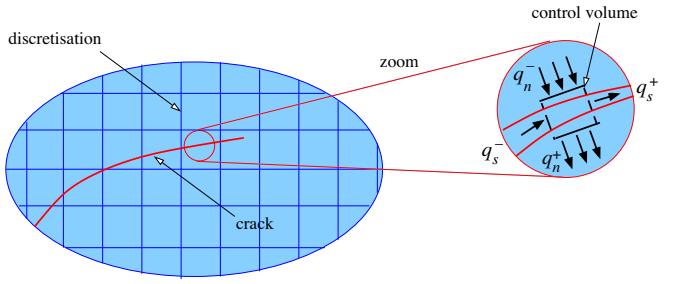

Fig. 1. Fluid-saturated porous medium with a crack and discretisation. The zoom shows the mass balance at sub-grid scale level.

A main thrust of this contribution is the classification of discretisation technologies for poroelastic interfaces, starting from the case that the pressure is continuous across the discontinuity, but where the pressure gradient is discontinuous. This relatively simple formulation already allows for the transport and storage of liquid inside the crack, provided that the pressure gradient can be discontinuous. In the extended finite element method this is achieved by partitioning the pressures at both sides of the discontinuity by a signed distance function [18,19]. In interface elements [24] a discontinuous pressure gradient across the discontinuity comes in naturally, as by definition they are $\mathcal{C}^0$-continuous with respect to the pressure across the interface. Pressure continuity has also been assumed by Armero and Callari [30] using a discontinuous enrichment for the displacements exploiting the Enhanced Assumed Strain concept. In the latter case flow and storage inside the cracks is *not* enabled since, within the element, the continuity of the pressure field is higher than $\mathcal{C}^0$.

Other poroelastic interfaces can be constructed starting from the assumption that the pressure is discontinuous orthogonal to the discontinuity [22,23,25,31], or that a Dirac function is superimposed on the interpolation functions for the pressure field as in [32]. Again, it depends on the applied discretisation technology whether flow and storage is enabled inside the crack. In [25,31] this has been achieved by partitioning the pressure field at both sides of the discontinuity through a Heaviside function placed at it, which enables the gradient to be discontinuous as well. Likewise, it is naturally embedded in interface elements with a double pressure node because of the $\mathcal{C}^{-1}$ continuity in the pressure field at the interface [22,23]. It is finally noted that (pressure-continuous) poroelastic interface elements have also been developed within the context of isogeometric analysis [33], including the possibility of fluid flow and storage in the discontinuity [34].

2. Fluid flow in a deformable porous medium

We consider a two-phase medium subject to the restriction of small variations in the concentrations and small displacement gradients, but it is noted that the extension to large displacement gradients has been considered [35]. Moreover, the treatment will be limited to a single fluid phase. This assumption has been made merely to avoid the complexities that would ensue otherwise. Indeed, the extension to a gas and a liquid phase is lengthy, but relatively straightforward [19,21], as is the extension towards thermo-hydro-mechanical modelling [36]. Finally, the assumptions are made that there is no mass transfer between the constituents and that the processes which we consider, occur isothermally. With these assumptions, the balances of linear momentum for the solid and the fluid phases read:

$$\nabla\cdot\boldsymbol{\sigma}_\pi + \hat{\mathbf{p}}_\pi + \rho_\pi \mathbf{g} = \frac{\partial(\rho_\pi \ \dot{\mathbf{u}}_\pi)}{\partial t} + \nabla\cdot(\rho_\pi \dot{\mathbf{u}}_\pi \otimes \dot{\mathbf{u}}_\pi) \tag{1}$$

with $\boldsymbol{\sigma}_\pi$ the stress tensor, ρ_π the apparent mass density, and $\dot{\mathbf{u}}_\pi$ the absolute velocity of constituent π. As in the remainder of this paper, $\pi = s, f$, where s and f denote the solid and fluid phases, respectively. The gravity acceleration is denoted by $\mathbf{g}$, and $\hat{\mathbf{p}}_\pi$ is the momentum source for constituent π from the other constituent. This takes into account the possible local drag interaction between the solid and the fluid. Evidently, the latter source terms must satisfy the momentum production constraint:

$$\sum_{\pi=s,f} \hat{\mathbf{p}}_\pi = \mathbf{0} \tag{2}$$

Neglecting convective, gravity and acceleration terms, the momentum balances reduce to:

$$\nabla\cdot\boldsymbol{\sigma}_\pi + \hat{\mathbf{p}}_\pi = \mathbf{0} \tag{3}$$

Adding both momentum balances, and taking into account Eq. (2), one obtains the momentum balance for the mixture:

$$\nabla\cdot\boldsymbol{\sigma} = \mathbf{0} \tag{4}$$

where we have for the total stress, as usual: $\boldsymbol{\sigma} = \boldsymbol{\sigma}_s + \boldsymbol{\sigma}_f$. With the Biot coefficient α, the total stress reads:

$$\boldsymbol{\sigma} = \boldsymbol{\sigma}_s - \alpha p \mathbf{I} \tag{5}$$

with p the fluid pressure and $\mathbf{I}$ the unit tensor.

Similarly, one can write the mass balance for each phase as:

$$\frac{\partial \rho_\pi}{\partial t} + \nabla\cdot(\rho_\pi \dot{\mathbf{u}}_\pi) = 0 \tag{6}$$

Consistent with the derivation of the momentum balance, variations in the mass density gradients are neglected, and the equations for the mass balance can be simplified to yield:

$$\frac{\partial \rho_\pi}{\partial t} + \rho_\pi \nabla\cdot\dot{\mathbf{u}}_\pi = 0 \tag{7}$$

Multiplying the mass balance for constituent π by its volumetric ratio n_π, summing the mass balances for the constituent phases, and utilising the constraint

$$\sum_{\pi=s,f} n_\pi = 1 \tag{8}$$

gives after some rewriting:

$$\nabla\cdot\dot{\mathbf{u}}_s + n_f \nabla\cdot(\dot{\mathbf{u}}_f - \dot{\mathbf{u}}_s) + \frac{n_s}{\rho_s}\frac{\partial \rho_s}{\partial t} + \frac{n_f}{\rho_f}\frac{\partial \rho_f}{\partial t} = 0 \tag{9}$$

Since it is reasonable to assume $K_t = n_s K_s$ for a nearly incompressible fluid, with K_s the bulk modulus of the solid material and K_t the overall bulk modulus of the porous medium, the mass balance for the solid constituent can be transformed into a relation between the change in the mass density of the solid material and its volume change:

$$\frac{K_s}{K_t}\ \frac{n_s}{\rho_s}\frac{\partial \rho_s}{\partial t} = -\nabla\cdot\dot{\mathbf{u}}_s \tag{10}$$

Using the Biot coefficient, $\alpha = 1 - K_t/K_s$ this equation can be written as:

$$(\alpha - 1)\nabla\cdot\dot{\mathbf{u}}_s = \frac{n_s}{\rho_s}\frac{\partial \rho_s}{\partial t} \tag{11}$$

For the fluid phase, a phenomenological relation is assumed between the rates of the apparent fluid mass density and the fluid pressure p:

$$\frac{n_f}{\rho_f}\frac{\partial \rho_f}{\partial t} = \frac{1}{Q}\frac{\partial p}{\partial t} \tag{12}$$

Please cite this article in press as: R. de Borst, Fluid flow in fractured and fracturing porous media: A unified view, Mech. Re. Commun. (2016), http://dx.doi.org/10.1016/j.mechrescom.2016.05.004

with Q the Biot modulus. The overall compressibility Q^{-1} can be related to the bulk modulus of the solid material, K_s, and the bulk modulus of the fluid, K_f, by [37]:

$$\frac{1}{Q}=\frac{\alpha-n_f}{K_s}+\frac{n_f}{K_f} \tag{13}$$

Inserting Eqs. (11) and (12) into the mass balance, Eq. (9), then gives:

$$\alpha\nabla\cdot\dot{\mathbf{u}}_s+n_f\nabla\cdot(\dot{\mathbf{u}}_f-\dot{\mathbf{u}}_s)+\frac{1}{Q}\frac{\partial p}{\partial t}=0 \tag{14}$$

The following boundary conditions need to be specified for the solid:

$$\mathbf{n}_\Gamma\cdot\boldsymbol{\sigma}=\mathbf{t}_p,\quad \dot{\mathbf{u}}_s=\dot{\mathbf{u}}_p \tag{15}$$

which hold on complementary parts of the boundary $\partial\Omega_t$ and $\partial\Omega_v$, with $\Gamma=\partial\Omega=\partial\Omega_t\cup\partial\Omega_v$, $\partial\Omega_t\cap\partial\Omega_v=\emptyset$. Herein, $\mathbf{t}_p$ is the prescribed external traction and $\dot{\mathbf{u}}_p$ is the prescribed velocity. Regarding the fluid, the boundary conditions

$$n_f(\dot{\mathbf{u}}_f-\dot{\mathbf{u}}_s)\cdot\mathbf{n}_\Gamma=q_p,\quad p=p_p \tag{16}$$

hold on complementary parts of the boundary $\partial\Omega_q$ and $\partial\Omega_p$, with $\Gamma=\partial\Omega=\partial\Omega_q\cup\partial\Omega_p$ and $\partial\Omega_q\cap\partial\Omega_p=\emptyset$, q_p and p_p being the prescribed outflow of pore fluid and the prescribed pressure, respectively. The initial conditions at $t=0$,

$$\mathbf{u}_\pi(\mathbf{x},0)=\mathbf{u}_\pi^0,\quad \dot{\mathbf{u}}_\pi(\mathbf{x},0)=\dot{\mathbf{u}}_\pi^0,\quad p(\mathbf{x},0)=p^0 \tag{17}$$

close the initial value problem.

3. Weak form of the balance equations

To arrive at the weak form of the balance equations, we multiply the momentum balance (4) and the mass balance (14) by kinetically admissible test functions for the displacements of the skeleton, $\boldsymbol{\eta}$, and for the pressure, ζ. Substituting Darcy's relation for the flow in the porous medium, e.g. [37]:

$$n_f(\dot{\mathbf{u}}_f-\dot{\mathbf{u}}_s)=-k_f\nabla p \tag{18}$$

with k_f the permeability of the bulk material, integrating over the domain Ω and using the divergence theorem then leads to the corresponding weak forms:

$$\int_\Omega(\nabla\cdot\boldsymbol{\eta})\cdot\boldsymbol{\sigma}\ \mathrm{d}\Omega+\int_{\Gamma_i}[\![\boldsymbol{\eta}\ \cdot\boldsymbol{\sigma}]\!]\cdot\mathbf{n}_{\Gamma_i}\ \mathrm{d}\Omega=\int_\Gamma\boldsymbol{\eta}\cdot\mathbf{t}_p\ \mathrm{d}\Omega \tag{19}$$

and

$$-\int_\Omega\alpha\zeta\nabla\cdot\dot{\mathbf{u}}_s\ \mathrm{d}\Omega+\int_\Omega k_f\nabla\zeta\cdot\nabla p\ \mathrm{d}\Omega-\int_\Omega\zeta Q^{-1}\dot{p}\ \mathrm{d}\Omega+\int_{\Gamma_i}\mathbf{n}_{\Gamma_i}\cdot[\![\zeta\ \ n_f(\dot{\mathbf{u}}_f-\dot{\mathbf{u}}_s)]\!]\ \mathrm{d}\Gamma=\int_\Gamma\zeta\mathbf{n}_\Gamma\cdot\mathbf{q}_p\ \mathrm{d}\Gamma \tag{20}$$

Because of the presence of a discontinuity inside the domain Ω, the power of the external tractions on Γ_i and the normal flux through the faces of the discontinuity are essential features of the weak formulation. Indeed, these terms enable the momentum and mass couplings between the discontinuity – the microscopic scale – and the surrounding porous medium – the macroscopic scale.

The momentum coupling stems from the tractions across the faces of the discontinuity and the pressure applied by the fluid in the discontinuity onto the faces of the discontinuity. We assume stress continuity from the cavity to the bulk, so that we have:

$$\boldsymbol{\sigma}\cdot\mathbf{n}_{\Gamma_i}=\mathbf{t}_i-p\mathbf{n}_{\Gamma_i} \tag{21}$$

with $\mathbf{t}_i$ the cohesive tractions, which vanish in case of a fully open crack. Hence, the weak form of the balance of momentum becomes:

$$\int_\Omega(\nabla\cdot\boldsymbol{\eta})\cdot\boldsymbol{\sigma}\ \mathrm{d}\Omega+\int_{\Gamma_i}[\![\boldsymbol{\eta}]\!]\cdot(\mathbf{t}_d-p\mathbf{n}_{\Gamma_i})\ \mathrm{d}\Gamma=\int_\Gamma\boldsymbol{\eta}\cdot\mathbf{t}_p\ \mathrm{d}\Gamma \tag{22}$$

Since the tractions have a unique value across the discontinuity, the pressure p must have the same value at both faces of the discontinuity, and, assuming a Bubnov–Galerkin approach, this must also hold for the test function for the pressure, ζ. Accordingly, the mass transfer coupling term for the liquid can be rewritten as follows:

$$-\int_\Omega\alpha\zeta\nabla\cdot\dot{\mathbf{u}}_s\ \mathrm{d}\Omega+\int_\Omega k_f\nabla\zeta\cdot\nabla p\ \mathrm{d}\Omega-\int_\Omega\zeta Q^{-1}\dot{p}\ \mathrm{d}\Omega+\int_{\Gamma_i}\zeta\mathbf{n}_{\Gamma_i}\cdot\mathbf{q}_i\mathrm{d}\Gamma=\int_\Gamma\zeta\mathbf{n}_\Gamma\cdot\mathbf{q}_p\ \mathrm{d}\Gamma \tag{23}$$

where

$$\mathbf{q}_i=n_f[\![\dot{\mathbf{u}}_f-\dot{\mathbf{u}}_s]\!] \tag{24}$$

represents the difference in the fluid fluxes through both faces of the interface.

4. A two-scale approach to fluid flow in a fractured porous medium

The flow of fluid in a fractured, or fracturing, porous medium consists of two subproblems: the flow in the cracks that separate the intact parts of the porous medium, and the interstitial flow in the pores of the intact parts of the medium. With respect to the former problem, we distinguish between two cases. First, fully open cracks are considered, where the flow is not disturbed. This case can be associated with linear elastic fracture mechanics, where no material exists in the cracks which can support possible (cohesive) tractions between both crack faces. For partially open cracks, cohesive zone models may be more appropriate, and it is plausible that there is material remaining in the cracks. In this case, the modelling of a crack as a porous medium, but of course with a different, usually much higher porosity, is conceivable.

4.1. Fluid flow in fully open cracks

Firstly, we assume an open cavity which is filled with a Newtonian fluid. The mass balance for the flow within the cavity reads:

$$\dot{\rho}_f+\rho_f\nabla\cdot\dot{\mathbf{u}}_f=0$$

subject to the assumptions of small changes in the concentrations and no convective terms, cf. Eq. (7). Furthermore, we assume that the first term can be neglected because there is only a single phase in the cavity so that the velocities are much higher than those in the surrounding porous medium. With this assumption the mass balance inside a two-dimensional cavity simplifies to:

$$\frac{\partial v}{\partial s}+\frac{\partial w}{\partial n}=0 \tag{25}$$

where $v=\dot{\mathbf{u}}_f\cdot\mathbf{t}_{\Gamma_i}$ and $w=\dot{\mathbf{u}}_f\cdot\mathbf{n}_{\Gamma_i}$ are the tangential and normal components of the fluid velocity in the discontinuity, respectively. $\mathbf{n}_{\Gamma_i}$ and $\mathbf{t}_{\Gamma_i}$ are the vectors normal and tangential to the discontinuity Γ_i, see Fig. 2, where the local s, n-coordinate system is also shown. The difference in the fluid velocity components that are normal to both crack faces is now given by:

$$[\![w_f]\!]=-\int_{n=-h}^{h}\frac{\partial v}{\partial s}\mathrm{d}n \tag{26}$$

Please cite this article in press as: R. de Borst, Fluid flow in fractured and fracturing porous media: A unified view, Mech. Re. Commun. (2016), http://dx.doi.org/10.1016/j.mechrescom.2016.05.004

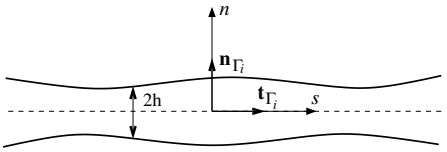

Fig. 2. Geometry and local coordinate system in cavity.

The momentum balance for the fluid in the s-direction reads:

$$\frac{\partial \tau}{\partial n} = \frac{\partial p}{\partial s} \tag{27}$$

with τ the shear stress. Together with the assumption of a Newtonian fluid,

$$\tau = \mu \frac{\partial v}{\partial n} \tag{28}$$

with μ the viscosity of the fluid, this gives:

$$\mu \frac{\partial^2 v}{\partial n^2} = \frac{\partial p}{\partial s} \tag{29}$$

After integration from $n=-h$ to $n=h$, a parabolic velocity profile results:

$$v(n) = \frac{1}{2\mu}\frac{\partial p}{\partial s}(n^2 - h^2) + v_f \tag{30}$$

where the essential boundary condition $v = v_f$ for the tangential velocity of the fluid has been applied at both faces of the cavity. Assuming a no-slip condition at the faces of the cavity, it stems from the relative fluid velocity in the porous medium at $n=\pm h$:

$$v_f = (\dot{u}_s - {n_f}^{-1} k_f \nabla p)\cdot \mathbf{t}_{\Gamma_i} \tag{31}$$

Substitution of Eq. (30) into Eq. (26) and again integrating with respect to n then leads to:

$$[\![w_f]\!] = \frac{2}{3\mu}\frac{\partial}{\partial s}\left(\frac{\partial p}{\partial s}h^3\right) - 2h\frac{\partial v_f}{\partial s} \tag{32}$$

This equation gives the amount of fluid attracted in the tangential fluid flow. Since

$$\frac{\partial (2h)}{\partial t} = [\![w_s]\!] \tag{33}$$

the mass coupling term becomes:

$$\mathbf{n}_{\Gamma_i}\cdot\mathbf{q}_d = n_f[\![w_f - w_s]\!] = n_f\left(\frac{2}{3\mu}\frac{\partial}{\partial s}\left(\frac{\partial p}{\partial s}h^3\right) - 2h\frac{\partial v_f}{\partial s} - 2\frac{\partial h}{\partial t}\right) \tag{34}$$

4.2. Fluid flow in partially open cracks

Linear elastic fracture mechanics applies when the area in which the dissipative processes take place remains small compared to the structural dimensions. When this requirement is not met, cohesive-zone models must be used [38–40]. Cohesive-zone models remove the stress and fluid pressure singularity that exists in linear elastic fracture mechanics [6]. Rice and Simons [41] have provided compelling arguments in favour of the use of cohesive-zone models by analysing shear crack growth in fluid-saturated porous media.

Considering the fact that the cavity is now partially filled with solid material, the initial value problem can be closed by assuming that the cavity is a porous material itself, of course with a different permeability than that of the surrounding bulk material. The mass balance for the fluid inside the cavity then reads:

$$\alpha_i \nabla\cdot\dot{u}_s + n_{fi}\nabla\cdot(\dot{u}_f - \dot{u}_s) + \frac{1}{Q_i}\frac{\partial p}{\partial t} = 0 \tag{35}$$

where the subscript i distinguishes quantities in the interface from those in the bulk. Because the width of the cavity $2h$ is negligible compared to its length, the mass balance is again enforced in an average sense over the cross section. For the first term, we can elaborate for a two-dimensional configuration:

$$\int_{n=-h}^{h}\alpha_i\nabla\cdot\dot{u}_s dn = \int_{n=-h}^{h}\alpha_i\left(\frac{\partial v_s}{\partial s} + \frac{\partial w_s}{\partial n}\right)dn = \int_{n=-h}^{h}\alpha_i\frac{\partial v_s}{\partial s}dn - \alpha_i[\![w_s]\!] \tag{36}$$

where v_s and w_s are the component of the solid velocity tangential and normal to the crack, respectively. Like the other constants (Q_i and n_{fi}), α_i has been assumed to be constant over the cross section. Also assuming that v_s varies linearly over the height of the cavity, and defining $\langle v_s\rangle = \frac{1}{2}(v_s(h) + v_s(-h))$, the integral can be solved analytically:

$$\int_{n=-h}^{h}\alpha_i\frac{\partial v_s}{\partial s}dn = 2\alpha_i h\langle\frac{\partial v_s}{\partial s}\rangle \tag{37}$$

Repeating these operations to the second term of Eq. (35), interchanging the order of integration and differentiation, and assuming that the boundary terms can be neglected, the following expression is obtained:

$$\int_{n=-h}^{h} n_{fi}\nabla\cdot(\dot{u}_f - \dot{u}_s)dn = n_{fi}[\![w_f - w_s]\!] + \frac{\partial}{\partial s}\left(\int_{-h}^{h} n_{fi}(v_f - v_s)dn\right) \tag{38}$$

We now introduce Darcy's relation in a one-dimensional sense in the direction of the crack,

$$n_{fi}(v_f - v_s) = -k_{si}\frac{\partial p}{\partial s} \tag{39}$$

with k_{si} the permeability of the damaged, porous material in the s-direction inside the cavity. In line with the preceding assumptions k_{si} is assumed not to depend on n. However, the decohesion inside the cavity is likely to affect the permeability, and therefore $k_{si} = k_{si}(h)$. Substituting Eq. (39) into Eq. (38), the following relation ensues:

$$\int_{n=-h}^{h} n_{fi}\nabla\cdot(\dot{u}_f - \dot{u}_s)dn = n_{fi}[\![w_f - w_s]\!] - \frac{\partial}{\partial s}\left(\int_{-h}^{h} k_{si}\frac{\partial p}{\partial s}dn\right) \tag{40}$$

so that:

$$\int_{-h}^{h} n_f\nabla\cdot(\dot{u}_f - \dot{u}_s)dn = n_f[\![w_f - w_s]\!] - 2h\frac{\partial k_{si}(h)}{\partial s}\frac{\partial p}{\partial s} - 2k_{si}h\frac{\partial^2 p}{\partial s^2} \tag{41}$$

Neglecting variations of the pressure over the height of the cavity, the third term can be elaborated as:

$$\int_{n=-h}^{h}\frac{1}{Q_i}\frac{\partial p}{\partial t}dy = \frac{2h}{Q_i}\frac{\partial p}{\partial t} \tag{42}$$

Since

$$n_{fi}[\![w_f - w_s]\!] \equiv \mathbf{n}_{\Gamma_i}\cdot\mathbf{q}_i \tag{43}$$

the coupling term becomes:

$$\mathbf{n}_{\Gamma_i}\cdot\mathbf{q}_i = -\frac{2h}{Q_i}\frac{\partial p}{\partial t} + 2\alpha_i\frac{\partial h}{\partial t} - 2\alpha_i h\langle\frac{\partial v_s}{\partial s}\rangle + 2h\frac{\partial k_{si}(h)}{\partial s}\frac{\partial p}{\partial s} + 2k_{si}h\frac{\partial^2 p}{\partial s^2} \tag{44}$$

Please cite this article in press as: R. de Borst, Fluid flow in fractured and fracturing porous media: A unified view, Mech. Re. Commun. (2016), http://dx.doi.org/10.1016/j.mechrescom.2016.05.004

4.3. Fluid flow with a pressure discontinuity in the normal direction

Storage and fluid flow in a direction that is tangential to the discontinuity, as described in the preceding two subsections, is possible when the pressure gradient orthogonal to the crack is discontinuous. The pressure can then still be assumed to be continuous. However, when this assumption is relaxed, so that the pressure itself can be discontinuous, for instance when having two pressure degrees of freedom at the crack, p^- and p^+, there can also be fluid transport across the discontinuity. This type of modelling has been pursued within the context of extended finite element methods in [25] and for interface elements in [22,23]. Defining the permeability for the fluid flow normal to the crack direction as k_{ni}, a discrete analogon of Darcy's relation can be postulated:

$$\mathbf{n}_{\Gamma_i} \cdot \mathbf{q}_i = -k_{ni}(p^+ - p^-) \tag{45}$$

Evidently, $k_{ni} = 0$ corresponds to an impervious boundary. For the limiting case that $k_{ni} \rightarrow \infty$ the case of a continuous pressure is retrieved ($p^+ = p^-$).

5. Interface elements

To accommodate discontinuities in finite element analysis, or considering Eqs. (22) and (23), to evaluate the integral at Γ_i, interface elements have found widespread use. Interface elements have to be inserted a priori in the finite element mesh. For stationary discontinuities, or when the direction of the propagation is known, interface elements can be used in a simple manner.

5.1. Interface kinematics

The kinematic quantities in continuous interface elements are a set of mutually orthogonal, relative displacements: $[\![u_n]\!]$, $[\![u_s]\!]$ for the normal and the sliding modes, respectively. For simplicity of notation, the discussion will be limited to two-dimensional configurations. The extension to three dimensions is straightforward, e.g. [42]. When collecting the relative displacements in a vector $[\![\mathbf{u}]\!]$, they can be related to the displacements at the upper (+) and the lower sides (−) of the interface, u_n^-, u_n^+, u_s^-, u_s^+, via

$$[\![\mathbf{u}]\!] = \mathrm{L}u \tag{46}$$

with

$$\mathbf{u}^{\mathrm{T}} = (u_n^-, u_n^+, u_s^-, u_s^+) \tag{47}$$

and

$$\mathbf{L} = \begin{bmatrix} -1 & +1 & 0 & 0 \\ 0 & 0 & -1 & +1 \end{bmatrix} \tag{48}$$

an operator matrix. For each side of the interface element, the displacements contained in $\mathbf{u}$ are interpolated in a standard manner as

$$\mathbf{u} = \mathbf{H}_u \mathbf{a} \tag{49}$$

with $\mathbf{a}$ the nodal displacement array,

$$\mathbf{a}^{\mathrm{T}} = \big((a_n^-)_1, \ldots, (a_n^-)_N, (a_s^-)_1, \ldots, (a_s^-)_N\ , \\ (a_n^+)_1, \ldots, (a_n^+)_N, (a_s^+)_1, \ldots, (a_s^+)_N\big) \tag{50}$$

and

$$\mathbf{H}_u = \begin{bmatrix} \mathbf{h}_u^{\mathrm{T}} & \mathbf{0} & \mathbf{0} & \mathbf{0} \\ \mathbf{0} & \mathbf{h}_u^{\mathrm{T}} & \mathbf{0} & \mathbf{0} \\ \mathbf{0} & \mathbf{0} & \mathbf{h}_u^{\mathrm{T}} & \mathbf{0} \\ \mathbf{0} & \mathbf{0} & \mathbf{0} & \mathbf{h}_u^{\mathrm{T}} \end{bmatrix} \tag{51}$$

with $\mathbf{h}_u$ a vector which contains the shape functions $(h_u)_1, \ldots, (h_u)_N$. The relation between the relative displacements in the interface elements and the nodal displacements reads:

$$[\![\mathbf{u}]\!] = \mathbf{L}\mathbf{H}_u\mathbf{a} = \mathbf{B}_u\mathbf{a} \tag{52}$$

with the relative displacement–nodal displacement matrix $\mathbf{B}_u$ for the interface element:

$$\mathbf{B}_u = \begin{bmatrix} -\mathbf{h}_u^{\mathrm{T}} & +\mathbf{h}_u^{\mathrm{T}} & \mathbf{0} & \mathbf{0} \\ \mathbf{0} & \mathbf{0} & -\mathbf{h}_u^{\mathrm{T}} & +\mathbf{h}_u^{\mathrm{T}} \end{bmatrix} \tag{53}$$

For an arbitrarily oriented interface element the matrix $\mathbf{B}_u$ must be transformed to the local coordinate system of the parent interface element.

5.2. Constitutive relation for the interface

Cohesive tractions $\mathbf{t}_i$ are related to the relative displacements $[\![\mathbf{u}]\!]$ via a nonlinear relation:

$$\mathbf{t}_i = \mathbf{t}_i([\![\mathbf{u}]\!], \kappa) \tag{54}$$

with κ a history parameter. For use in a Newton–Raphson iterative procedure this constitutive relation can be linearised as:

$$\mathrm{d}\mathbf{t}_i = \mathbf{D}_i \mathrm{d}[\![\mathbf{u}]\!] \tag{55}$$

with d a small increment, and

$$\mathbf{D}_i = \frac{\partial \mathbf{t}_i}{\partial [\![\mathbf{u}]\!]} \tag{56}$$

Interface elements have to be inserted in the finite element mesh at the beginning of the computation, and therefore, a finite stiffness must be assigned in the pre-cracking phase with at least the diagonal elements being non-zero. Prior to crack initiation, the material tangential stiffness matrix in the interface element therefore reads:

$$\mathbf{D}_i = \begin{bmatrix} d_n & 0 \\ 0 & d_s \end{bmatrix} \tag{57}$$

with d_n and d_s high values for the normal and tangential stiffnesses, respectively, which should be taken as high as possible in order to minimise the non-physical compliance due to this term prior to crack initiation. However, very high values may result in traction oscillations, which can be remedied by replacing Gauss integration by Newton-Cotes integration of the interface terms [43].

6. Poromechanical interface elements

For the pressure we distinguish between a continuous pressure (one pressure node), a discontinuous pressure (two pressure nodes), and the case that the fluid pressure in the cavity is different from that in the bulk material. When assuming that the pressure in the bulk at both sides of the crack is the same, two pressure degrees of freedom suffice. This assumption is identical to the pressure enhancement proposed in [32] in the context of embedded strong discontinuities formulated within the framework of the Enhanced Assumed Strain concept. In that case, a pressure in the form of a Dirac function was superimposed on a smoothly varying pressure

Please cite this article in press as: R. de Borst, Fluid flow in fractured and fracturing porous media: A unified view, Mech. Re. Commun. (2016), http://dx.doi.org/10.1016/j.mechrescom.2016.05.004

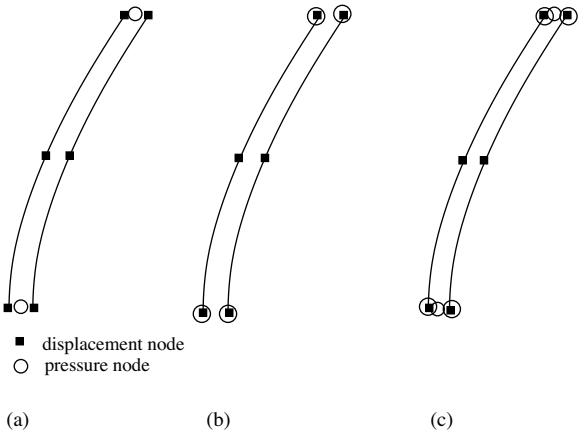

Fig. 3. Two-dimensional interface elements enriched with pressure nodes.

field within an element. However, from a physical point of view the case that the pressure is the same at both sides of the interface is probably less relevant, and its treatment is not pursued here. When the pressures at both sides of the crack are allowed to differ, a three-pressure node model in the spirit of [44] ensues.

It is noted that the pressure gradient can be discontinuous in all cases, thus allowing for storage and fluid flow within the discontinuity, since the pressure across the interface element is at most interpolated with $\mathcal{C}^0$-continuity.

6.1. Continuous pressure

We first consider the case of a continuous pressure across the interface element, so that there is a single pressure node only, Fig. 3(a). The pressure in the interface is then interpolated as:

$$p = \mathbf{h}_p^{\mathrm{T}}\mathbf{p} \tag{58}$$

where $\mathbf{h}_p$ is a vector that contains the interpolation polynomials $(h_p)_1, \ldots, (h_p)_N$ for the pressure, and

$$\mathbf{p}^{\mathrm{T}} = (p_1, \ldots, p_N) \tag{59}$$

contains the nodal values of the pressure p. We discretise the test functions $\boldsymbol{\eta}$ and ζ for the displacement and the pressure, respectively, in a Bubnov–Galerkin sense:

$$\boldsymbol{\eta} = \mathbf{H}_u\mathbf{w}, \quad \zeta = \mathbf{h}_p^{\mathrm{T}}\mathbf{z} \tag{60}$$

with $\mathbf{w}$ and $\mathbf{z}$ the corresponding nodal arrays. Using Eq. (52) the mechanical interface term in the weak form of the momentum balance, Eq. (22), can subsequently be elaborated as follows:

$$\int_{\Gamma_i} [\![\boldsymbol{\eta}]\!]\cdot(\mathbf{t}_i - p\mathbf{n}_{\Gamma_i})\mathrm{d}\Gamma = \int_{\Gamma_i} \mathbf{w}^{\mathrm{T}}\mathbf{B}_u^{\mathrm{T}}(\mathbf{t}_i - p\mathbf{n}_{\Gamma_i}) \ \mathrm{d}\Gamma \tag{61}$$

and the contribution to the internal force vector reads:

$$\mathbf{f}_u^{\mathrm{int}} = \int_{\Gamma_i} \mathbf{B}_u^{\mathrm{T}}(\mathbf{t}_i - p\mathbf{n}_{\Gamma_i}) \ \mathrm{d}\Gamma \tag{62}$$

Using Eqs. (52), (55) and (58) the contributions to the tangential stiffness matrix become:

$$\frac{\partial \mathbf{f}_u^{\mathrm{int}}}{\partial \mathbf{a}} = \int_{\Gamma_i} \mathbf{B}_u^{\mathrm{T}}\mathbf{D}_i\mathbf{B}_u\mathrm{d}\Gamma \tag{63}$$

and

$$\frac{\partial \mathbf{f}_u^{\mathrm{int}}}{\partial \mathbf{p}} = -\int_{\Gamma_i} \mathbf{B}_u^{\mathrm{T}}\mathbf{n}_{\Gamma_i}\mathbf{h}_p^{\mathrm{T}}\mathrm{d}\Gamma \tag{64}$$

The interface term in the weak form of the mass balance can be elaborated as:

$$\int_{\Gamma_i} \zeta\mathbf{n}_{\Gamma_i}\cdot\mathbf{q}_i\mathrm{d}\Gamma = \mathbf{z}^{\mathrm{T}}\int_{\Gamma_i} \mathbf{h}_p\mathbf{n}_{\Gamma_i}^{\mathrm{T}}\mathbf{q}_i\mathrm{d}\Gamma \tag{65}$$

and the contribution of interface term in the mass balance to internal force vector reads:

$$\mathbf{f}_p^{\mathrm{int}} = \int_{\Gamma_i} \mathbf{h}_p\mathbf{n}_{\Gamma_i}^{\mathrm{T}}\mathbf{q}_i\mathrm{d}\Gamma \tag{66}$$

Since the flux at the interface $\mathbf{q}_i = \mathbf{q}_i\left([\![u]\!], p\right)$, cf. Eqs. (34) and (44), two contributions from this term to the tangential stiffness matrix ensue:

$$\frac{\partial \mathbf{f}_p^{\mathrm{int}}}{\partial \mathbf{a}} = \int_{\Gamma_i} \mathbf{h}_p\mathbf{n}_{\Gamma_i}^{\mathrm{T}}\frac{\partial \mathbf{q}_i}{\partial [\![\mathbf{u}]\!]}\mathbf{B}_u\mathrm{d}\Gamma \tag{67}$$

and

$$\frac{\partial \mathbf{f}_p^{\mathrm{int}}}{\partial \mathbf{p}} = \int_{\Gamma_i} \mathbf{h}_p\mathbf{n}_{\Gamma_i}^{\mathrm{T}}\frac{\partial \mathbf{q}_i}{\partial p}\mathbf{h}_p^{\mathrm{T}}\mathrm{d}\Gamma \tag{68}$$

It is noted that, together with the interface terms that stem from the linearisation of the momentum balance, these terms render the tangential stiffness matrix non-symmetric.

6.2. Discontinuous pressure

In case of a possible discontinuous pressure across the interface element, i.e. when there are two pressure nodes, Fig. 3(b), the fluid flux in the interface reads, cf. Eq. (45):

$$\mathbf{n}_{\Gamma_i}\cdot\mathbf{q}_i = -k_{ni}[\![p]\!] = -k_{ni}\mathbf{l}^{\mathrm{T}}\mathbf{H}_p\mathbf{p} \tag{69}$$

with

$$\mathbf{l}^{\mathrm{T}} = [\,-1 \quad +1\,] \tag{70}$$

$$\mathbf{H}_p = \begin{bmatrix} \mathbf{h}_p^{\mathrm{T}} & \mathbf{0} \\ \mathbf{0} & \mathbf{h}_p^{\mathrm{T}} \end{bmatrix} \tag{71}$$

and $\mathbf{p}$ *now* defined as:

$$\mathbf{p}^{\mathrm{T}} = \left((p^-)_1, \ldots, (p^-)_N, (p_+)_1, \ldots, (p^+)_N\right) \tag{72}$$

Defining the $1 \times 2N$-matrix

$$\mathbf{B}_p = \left[\,-\mathbf{h}_p \quad \mathbf{h}_p\,\right] \tag{73}$$

one can also write

$$\mathbf{n}_{\Gamma_i}\cdot\mathbf{q}_i = -k_{ni}\mathbf{B}_p\mathbf{p} \tag{74}$$

An anomaly of the approach is that there is no (separate) pressure within the interface. As a consequence, the pressure vanishes from the stress continuity condition across the interface to become:

$$\boldsymbol{\sigma}\cdot\mathbf{n}_{\Gamma_i} = \mathbf{t}_i \tag{75}$$

and, instead of Eq. (62), we have for the interface contribution to the internal force vector:

$$\mathbf{f}_u^{\mathrm{int}} = \int_{\Gamma_i} \mathbf{B}_u^{\mathrm{T}}\mathbf{t}_i \ \mathrm{d}\Gamma \tag{76}$$

Since in the absence of an interface pressure p, $\mathbf{f}_u^{\mathrm{int}}$ can no longer depend on it, the interface stiffness term $\frac{\partial \mathbf{f}_u^{\mathrm{int}}}{\partial \mathbf{p}}$ cancels as well, and only the interface stiffness $\frac{\partial \mathbf{f}_u^{\mathrm{int}}}{\partial \mathbf{a}}$ remains.

Please cite this article in press as: R. de Borst, Fluid flow in fractured and fracturing porous media: A unified view, Mech. Re. Commun. (2016), http://dx.doi.org/10.1016/j.mechrescom.2016.05.004

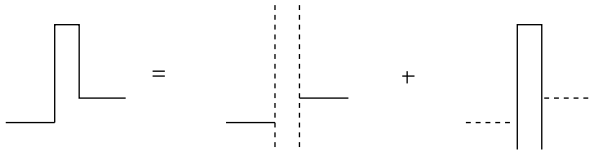

Fig. 4. Pressures across the interface for an enriched discontinuous pressure model.

Similarly, the interface term in the mass matrix simplifies, and substituting Eq. (74) into Eq. (65), the contribution of interface term in the mass balance to internal force vector becomes:

$$\mathbf{f}_p^{\text{int}} = -\left(\int_{\Gamma_i} k_{ni}\mathbf{h}_p\mathbf{B}_p \mathrm{d}\Gamma\right)\mathbf{p} \tag{77}$$

and the only non-vanishing contribution from the interface to the tangential stiffness matrix becomes:

$$\frac{\partial \mathbf{f}_p^{\text{int}}}{\partial \mathbf{p}} = -\int_{\Gamma_i} k_{ni}\mathbf{h}_p\mathbf{B}_p \mathrm{d}\Gamma \tag{78}$$

6.3. Discontinuous pressure with independent pressure in the interface

The deficiency of the discontinuous pressure model can be remedied by superimposing a (regularised) Dirac function for the pressure, in the spirit of the local enrichment proposed by [32], see Fig. 4. The independent pressures are now p^- at the Γ_i^--side of the interface Γ_i, p^+ at the Γ_i^+-side and p_i within the interface. Clearly, the existence of an independent pressure within the discontinuity allows for modelling pressurising the crack, which permits extension of the modelling capabilities to hydraulic fracturing.

Different from the previous two cases, an explicit distinction must now be made between the inflow of liquid through Γ^- and Γ^+-sides. In principle, the resistance at both boundaries can be different, and (time-dependent) expressions for leak-off have been derived based on a heat conduction analogy [44]. For simplicity we will not pursue this herein, and postulate the following relation between the flux into the discontinuity and the pressures:

$$\mathbf{n}_{\Gamma_i}\cdot\mathbf{q}_i = -k_{ni}(p^- - p_i) - k_{ni}(p^+ - p_i) = k_{ni}(2p_i - p^+ - p^-) \tag{79}$$

With (p^-, p^+) interpolated as

$$\begin{pmatrix} p^- \\ p^+ \end{pmatrix} = \mathbf{H}_p\mathbf{p} \tag{80}$$

cf. Eqs. (71) and (72), and a separate interpolation for p_i:

$$p_i = \mathbf{h}_i^{\mathrm{T}}\mathbf{p}_i \tag{81}$$

where the vector $\mathbf{h}_i$ holds the interpolation functions for the pressure within the interface and $\mathbf{p}_i$ contains the nodal values. Noting that

$$p^- + p^+ = (1 \quad 1)\,\mathbf{H}_p\mathbf{p} \tag{82}$$

where Eqs. (71) and (72) have been invoked, and defining

$$\mathbf{b}_p^{\mathrm{T}} = (1, \quad 1)\,\mathbf{H}_p \tag{83}$$

Eq. (79) can be rewritten as:

$$\mathbf{n}_{\Gamma_i}\cdot\mathbf{q}_i = 2k_{ni}\mathbf{h}_i^{\mathrm{T}}\mathbf{p}_i - k_{ni}\mathbf{b}_p^{\mathrm{T}}\mathbf{p} \tag{84}$$

Different from the case with the two pressure nodes, there is now a pressure p_i within the crack. The contribution of the interface to the part of the internal force vector that stems from the momentum balance therefore remains as in the single pressure model,

$$\mathbf{f}_u^{\text{int}} = \int_{\Gamma_i} \mathbf{B}_u^{\mathrm{T}}(\mathbf{t}_i - p_i\mathbf{n}_{\Gamma_i})\ \mathrm{d}\Gamma$$

cf. Eq. (62), and using Eqs. (52), (55) and (81) the contributions to the tangential stiffness matrix become:

$$\frac{\partial \mathbf{f}_u^{\text{int}}}{\partial \mathbf{a}} = \int_{\Gamma_i} \mathbf{B}_u^{\mathrm{T}}\mathbf{D}_i\mathbf{B}_u \mathrm{d}\Gamma \tag{85}$$

and

$$\frac{\partial \mathbf{f}_u^{\text{int}}}{\partial \mathbf{p}_i} = -\int_{\Gamma_i} \mathbf{B}_u^{\mathrm{T}}\mathbf{n}_{\Gamma_i}\mathbf{h}_i^{\mathrm{T}} \mathrm{d}\Gamma \tag{86}$$

where the total array of unknowns reads:

$$\begin{pmatrix} \mathbf{a} \\ \mathbf{p} \\ \mathbf{p}_i \end{pmatrix} \tag{87}$$

The interface term in the weak form of the mass balance now results in two contributions to the total internal force vector:

$$\int_{\Gamma_i} \zeta\mathbf{n}_{\Gamma_i}\cdot\mathbf{q}_i \mathrm{d}\Gamma + \int_{\Gamma_i} \zeta_i\mathbf{n}_{\Gamma_i}\cdot\mathbf{q}_i \mathrm{d}\Gamma$$
$$= \mathbf{z}^{\mathrm{T}}\int_{\Gamma_i} \mathbf{H}_p^{\mathrm{T}}\mathbf{n}_{\Gamma_i}^{\mathrm{T}}\mathbf{q}_i \mathrm{d}\Gamma + \mathbf{z}_i^{\mathrm{T}}\int_{\Gamma_i} \mathbf{h}_i\mathbf{n}_{\Gamma_i}^{\mathrm{T}}\mathbf{q}_i \mathrm{d}\Gamma \tag{88}$$

where ζ_i the test function for p_i, and $\mathbf{z}_i$ contains the corresponding nodal values. Inserting Eq. (84) then results in:

$$\int_{\Gamma_i} \zeta\mathbf{n}_{\Gamma_i}\cdot\mathbf{q}_i \mathrm{d}\Gamma + \int_{\Gamma_i} \zeta_i\mathbf{n}_{\Gamma_i}\cdot\mathbf{q}_i \mathrm{d}\Gamma$$
$$= \mathbf{z}^{\mathrm{T}}\int_{\Gamma_i} \mathbf{H}_p^{\mathrm{T}}\left(2k_{ni}\mathbf{h}_i^{\mathrm{T}}\mathbf{p}_i - k_{ni}\mathbf{b}_p^{\mathrm{T}}\mathbf{p}\right)\mathrm{d}\Gamma + \mathbf{z}_i^{\mathrm{T}}\int_{\Gamma_i} \mathbf{h}_i\left(2k_{ni}\mathbf{h}_i^{\mathrm{T}}\mathbf{p}_i - k_{ni}\mathbf{b}_p^{\mathrm{T}}\mathbf{p}\right)\mathrm{d}\Gamma \tag{89}$$

The contributions of interface term in the mass balance to internal force vector then read:

$$\mathbf{f}_p^{\text{int}} = \left(\int_{\Gamma_i} 2k_{ni}\mathbf{H}_p^{\mathrm{T}}\mathbf{h}_i^{\mathrm{T}} \mathrm{d}\Gamma\right)\mathbf{p}_i - \left(\int_{\Gamma_i} k_{ni}\mathbf{H}_p^{\mathrm{T}}\mathbf{b}_p^{\mathrm{T}} \mathrm{d}\Gamma\right)\mathbf{p} \tag{90}$$

and

$$\mathbf{f}_{p_i}^{\text{int}} = \left(\int_{\Gamma_i} 2k_{ni}\mathbf{h}_i\mathbf{h}_i^{\mathrm{T}} \mathrm{d}\Gamma\right)\mathbf{p}_i - \left(\int_{\Gamma_i} k_{ni}\mathbf{h}_i\mathbf{b}_p^{\mathrm{T}} \mathrm{d}\Gamma\right)\mathbf{p} \tag{91}$$

The contributions to the tangential stiffness matrix can subsequently be derived to be:

$$\frac{\partial \mathbf{f}_p^{\text{int}}}{\partial \mathbf{p}} = -\int_{\Gamma_i} k_{ni}\mathbf{H}_p^{\mathrm{T}}\mathbf{b}_p^{\mathrm{T}} \mathrm{d}\Gamma, \quad \frac{\partial \mathbf{f}_p^{\text{int}}}{\partial \mathbf{p}_i} = \int_{\Gamma_i} 2k_{ni}\mathbf{H}_p^{\mathrm{T}}\mathbf{h}_i^{\mathrm{T}} \mathrm{d}\Gamma \tag{92}$$

and

$$\frac{\partial \mathbf{f}_{p_i}^{\text{int}}}{\partial \mathbf{p}} = -\int_{\Gamma_i} k_{ni}\mathbf{h}_i\mathbf{b}_p^{\mathrm{T}} \mathrm{d}\Gamma, \quad \frac{\partial \mathbf{f}_{p_i}^{\text{int}}}{\partial \mathbf{p}} = \int_{\Gamma_i} 2k_{ni}\mathbf{h}_i\mathbf{h}_i^{\mathrm{T}} \mathrm{d}\Gamma \tag{93}$$

7. Extended finite element method

The extended finite element method [45,46] can be viewed as a generalisation of interface elements which can be put arbitrarily within elements. Indeed, when the discontinuity is aligned with

Please cite this article in press as: R. de Borst, Fluid flow in fractured and fracturing porous media: A unified view, Mech. Re. Commun. (2016), http://dx.doi.org/10.1016/j.mechrescom.2016.05.004

an element edge, the standard interface element formulation is retrieved [42,47].

Since finite element shape functions h_j form partitions of unity, $\sum_{j=1}^{N} h_j = 1$ with N the number of nodal points, the components u_i of a displacement field $\mathbf{u}$ can be interpolated as [48]:

$$u_i = \sum_{j=1}^{N} h_j \left(\bar{a}_j + \sum_{k=1}^{M} \psi_k \hat{a}_{jk} \right) \tag{94}$$

with $\bar{a}_j$ the regular nodal degrees-of-freedom for the displacements, ψ_k enhanced basis terms, and $\hat{a}_{jk}$ additional displacement degrees-of-freedom at node j which represent the amplitude of the kth enhanced basis term ψ_k. We consider a domain Ω that is crossed by a single discontinuity at Γ_i. The displacement field $\mathbf{u}$ is then written as the sum of two continuous displacement fields $\bar{\mathbf{u}}$ and $\hat{\mathbf{u}}$:

$$\mathbf{u} = \bar{\mathbf{u}} + \mathcal{H}_{\Gamma_i} \hat{\mathbf{u}} \tag{95}$$

with $\mathcal{H}_{\Gamma_i}$ the Heaviside step function centred at the discontinuity. The decomposition in Eq. (95) has a structure similar to the interpolation in Eq. (94). Accordingly, the partition-of-unity property of finite element shape functions enables the direct incorporation of discontinuities, including cracks and shear bands, in finite element models such that the discontinuous character of cracks and shear bands is preserved.

With respect to the interpolation of the pressure p we note that, different from interface elements, the discontinuity can be anywhere in the element, so that normally it does not coincide with a $\mathcal{C}^0$-continuity line. In fact, only when the discontinuity is put at an edge of the element, such a $\mathcal{C}^0$-continity line in the interpolation of the pressure field would coincide with the discontinuity. This implies that within the framework of the extended finite element method, a $\mathcal{C}^0$-line must be enforced. The simplest way to do so is to partition the pressure field as

$$p = \bar{p} + \mathcal{D}_{\Gamma_i} \hat{p} \tag{96}$$

with the distance function $\mathcal{D}_{\Gamma_i}$ defined as:

$$\mathbf{n}_{\Gamma_i} \cdot \nabla \mathcal{D}_{\Gamma_i} = \mathcal{H}_{\Gamma_i} \tag{97}$$

This corresponds to an interface element with a single pressure node, hence the pressure gradient normal to the discontinuity is discontinuous. Since the fluid velocity is proportional to the pressure gradient via Darcy's relation, this quantity is discontinuous as well. Alternatively we can partition the pressure field as:

$$p = \bar{p} + \mathcal{H}_{\Gamma_i} \hat{p} \tag{98}$$

Then, the pressure field can be discontinuous across the interface in addition to the pressure gradient, and we retrieve the model of an interface element with a double pressure node. An extended finite element formulation that corresponds with a pressure inside the discontinuity that is different from that in the surrounding bulk material, i.e. the three pressure node formulation of interface elements, is less natural, but has achieved by Remij et al. [44].

As an example, a square-shaped fractured block is considered under plane-strain conditions. A set of ten randomly generated, stationary open faults is considered in a linear-elastic medium and no tractions are transferred between both sides of each crack. The sub-grid scale model for the fluid flow in an open cavity is used together with the distance function interpolation for the pressure, Eq. (97), and singularity functions that stem from linear-elastic fracture mechanics are added as enrichment functions at the crack tips [18]. A normal fluid flux $q_0 = 10^{-4}$ ms^{-1} starting at $t = 0$ s is imposed at the bottom, while the top face is assigned a drained condition with zero pressure. The left and the right face are assumed to be undrained. No mechanical load is applied, and essential boundary conditions have been applied to remove rigid body motions. The

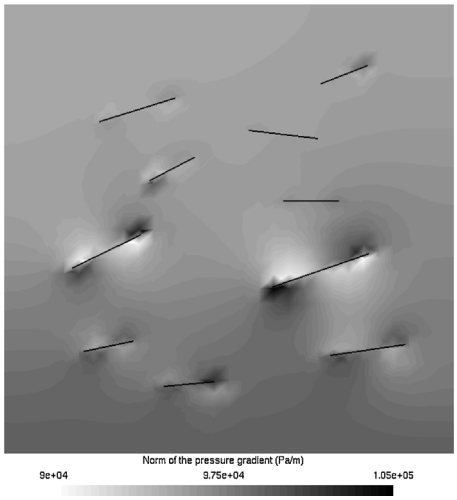

Fig. 5. L_2 – Norm of the pressure gradient.

dimensions of the block are 10 m × 10 m. The porous material has a fluid volume fraction $n_f = 0.3$ and a permeability $k_f = 10^{-9}$ m^3/Ns. The Young's modulus $E = 9$ GPa and Poisson's ratio $\nu = 0.40$. The Biot coefficient $\alpha = 1$, and the Biot modulus has been assigned a value $Q = 10^{18}$ GPa to simulate a quasi-incompressible fluid.

The length of the faults is between 1 and 3 m, while the fault angles vary from -10° to $+30^\circ$. Fig. 5 shows the influence of the faults on the norm of the pressure gradient. The global fluid flow is strongly affected by the fluid flow inside the faults. From Fig. 5 it is observed that the main effect is due to the two longest faults. Evidently, the effect of a fault on the macroscopic flow increases with its length because more fluid can flow inside the cavity.

8. Isogeometric interface elements

A fourth discretisation technology that allows for simulating poromechanical fracture problems is isogeometric finite element analysis [49]. The flexibility in capturing complex domains, and, probably even more importantly, the inherent higher-order continuity that is advantageous when dealing with higher-order derivatives, are very promising and appealing.

In [50] the ability of isogeometric finite elements to simulate cohesive fracture has been demonstrated. While issues pertain with crack propagation in arbitrary directions and crack branching, it has been shown in [33] that isogeometric interface elements can be efficient and highly accurate for stationary poromechanical fracture problems. In [34] the concept has been extended to transport and storage of fluid flow in existing cracks, while also introducing different orders of interpolation for the continuum isogeometric two-phase elements that surround the discontinuity.

The formulation of isogeometric interface elements is relatively straightforward. It essentially consists of replacing the traditional Lagrangian interpolation functions by B-spline functions, and using Bézier extraction in order to arrive at an element concept that fits standard data structures. Then, the operations to form the internal force vector and the tangential stiffness become identical to that of a standard interface as formulated above, cf. [33]. It is noted, however, that the traction oscillations exhibited by standard interface elements become even worse in case of isogeometric interface elements [43,51], and different from standard interface elements, do not disappear when Gauss integration is replaced by Newton–Cotes integration. Only lumped integration seems to be an adequate remedy.

As an example, the square block of Fig. 6 is considered. It is crossed by a discontinuity inclined at an angle α. The central part

Please cite this article in press as: R. de Borst, Fluid flow in fractured and fracturing porous media: A unified view, Mech. Re. Commun. (2016), http://dx.doi.org/10.1016/j.mechrescom.2016.05.004

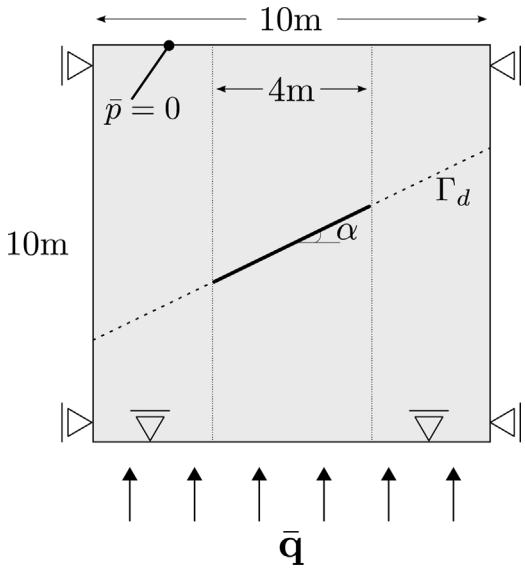

Fig. 6. Geometry of a square plate crossed by an interface with an inclined crack.

of Γ_i is traction free. A quasi-incompressible fluid is considered with $Q = 10^{18}$ MPa. The Young's modulus is taken as $E = 9 \times 10^3$ MPa and the Poisson ratio is assumed as $\nu = 0.4$. The dummy stiffnesses at the interface are chosen as $d_n = d_s = 10^5$ MPa. The hydraulic permeability is taken as $k_f = 10^3$ mm^4 N^{-1} s^{-1}, the fluid viscosity as $\mu = 10^{-9}$ Nm m^{-2} s^{-1}, and the porosity as $n_f = 0.3$.

Figs. 8 and 9 show the effect of the flow in the cavity on the area surrounding the cavity at an early stage of the simulation. When the term for the flow in the discontinuity is made inactive, the flux is the same at both faces of the discontinuity. The absence of a flux jump implies that the fluid flows through the cavity without being affected by it. The jump in the fluid flow is clearly visibly in Fig. 9,

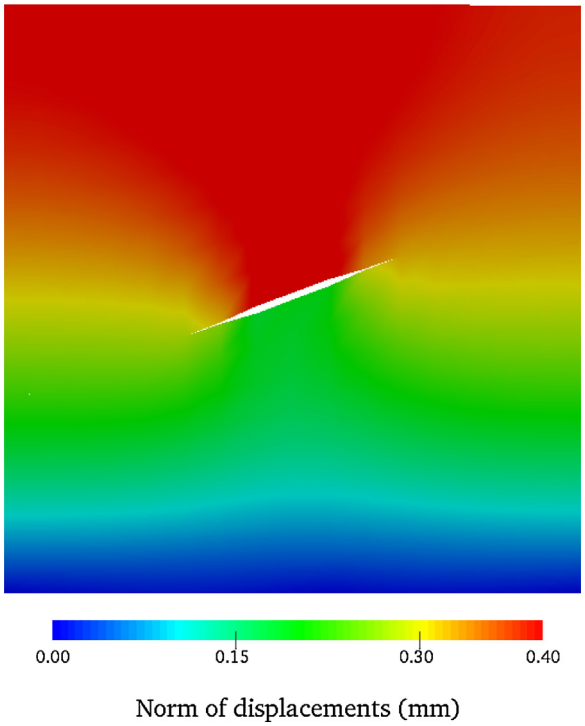

Fig. 7. Contour plot of displacements for the steady state of a square plate crossed by an interface (magnification factor 500).

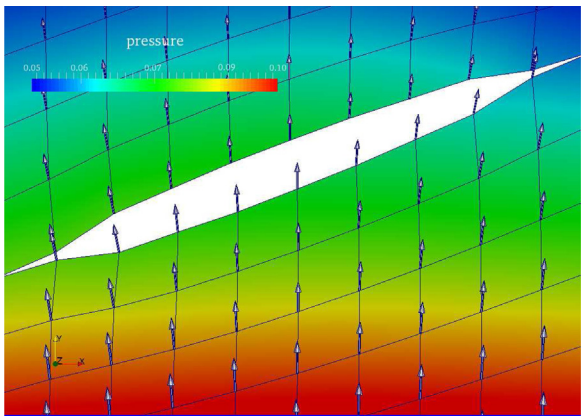

Fig. 8. Pressure contours and flux vectors near the cavity at $t = 1$ s for the case of no flow in the cavity.

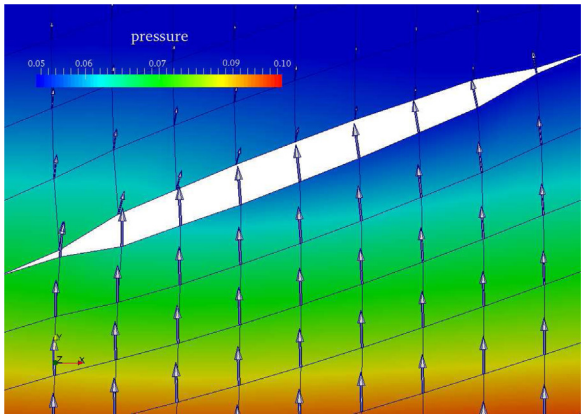

Fig. 9. Pressure contours and flux vectors near the cavity at $t = 1$ s when flow in the cavity is included.

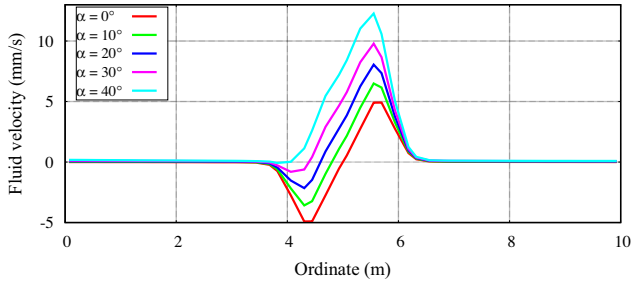

Fig. 10. Tangential fluid velocity along the interface at steady state.

due to the fact that fluid is stored (because of crack opening) and is flowing away within the cavity.

Fig. 10 shows that for an horizontal crack ($\alpha = 0$), the fluid velocity is symmetric in the cavity, flowing to the left and to the right with equal magnitudes. When the interface is inclined, the fluid can accelerate in the cavity, which starts to behave like a resistance-free channel for the fluid.

9. Concluding remarks

Sub-grid scale models for fluid flow and storage in cracks that intersect a porous medium have been summarised. It has been argued that the models are universal in the sense that they can be embedded in different discretisation strategies, e.g. interface elements, extended finite elements, and isogeometric finite element

Please cite this article in press as: R. de Borst, Fluid flow in fractured and fracturing porous media: A unified view, Mech. Re. Commun. (2016), http://dx.doi.org/10.1016/j.mechrescom.2016.05.004

analysis. Examples have been given to demonstrate the potential of the approach. Next, a family of poromechanical interface elements has been described, with single, double and triple pressure nodes at the interface. The physical consequences of the different assumptions have been elucidated, and it has been shown how existing approaches fit within the framework. While the categorisation has been done for classical interface elements, it also holds for other discretisation techniques, like extended finite elements and isogeometric finite element analysis.

Which discretisation technique is preferred, depends on the application. When cracks are stationary and/or their location is known, interface elements are sufficiently general, and have the advantage of being simple to formulate and implement. Indeed, they are available at a wide scale. For arbitrary crack propagation, one must either use extended finite element methods or remeshing. While the former technique is perhaps more elegant, the latter technique can be more accurate, as it allows placing nodes, and hence additional degrees of freedom close to the crack tips, thus ensuring the computation of a more accurate stress field locally. In complicated geometries, as encountered in engineering practice, this may be an advantage. In addition, powerful mesh generators are nowadays widely available. Finally, isogeometric analysis is perhaps the most complicated method, definitely not yet so broadly accepted, although Bézier extraction, which allows to cast the method into a standard finite element format, is rapidly changing this picture. A major advantage is the higher-order continuity, which allows much more accurate computation of gradients, thus leading to much more accurate stress fields around crack tips, but also automatically ensuring mass balance at interelement boundaries [52].

Acknowledgements

Financial support through the ERC Advanced Grant 664734 “PoroFrac” is gratefully acknowledged.

References

[1] T.K. Perkins, L.R. Kern, Widths of hydraulic fractures, J. Pet. Technol. 13 (1961) 937–949.
[2] R.P. Nordgren, Propagation of a vertical hydraulic fracture, SPE J. 12 (1972) 306–314.
[3] S.A. Khristianovic, Y.P. Zheltov, Formation of vertical fractures by means of highly viscous fluids., in: Proceedings Fourth World Petroleum Congress, Rome, 1955, pp. 579–586.
[4] J. Geertsma, F. de Klerk, A rapid method of predicting width and extent of hydraulically induced fractures, J. Pet. Technol. 21 (1969) 1571–1581.
[5] R.D. Carter, Optimum fluid characteristics for fracture extension., in: Drilling and Production Practices No. 57, API, Tulsa, Oklahoma, 1957, pp. 261–270.
[6] E. Detournay, Propagation regimes of fluid-driven fractures in impermeable rocks, J. Geomech. 4 (2004) 35–45.
[7] G.I. Barenblatt, I.P. Zheltzov, I.N. Kochina, Basic concepts in the theory of seepage of homogeneous liquids in fissured rocks, J. Appl. Math. 24 (1960) 1286–1303.
[8] E.C. Aifantis, On the problem of diffusion in solids, Acta Mech. 37 (1980) 265–296.
[9] R.K. Wilson, E.C. Aifantis, On the theory of consolidation with double porosity – III. A finite element formulation, Int. J. Eng. Sci. 20 (1982) 1009–1035.
[10] M.Y. Khaled, D.E. Beskos, E.C. Aifantis, On the theory of consolidation with double porosity – III. A finite element formulation, Int. J. Numer. Anal. Methods Geomech. 8 (1984) 101–123.
[11] M.A. Biot, General theory of three-dimensional consolidation, J. Appl. Phys. 12 (1941) 155–164.
[12] T.J. Boone, A.R. Ingraffea, A numerical procedure for simulation of hydraulic-driven fracture propagation in poroelastic media, Int. J. Numer. Anal. Methods Geomech. 14 (1990) 27–47.
[13] B.J. Carter, J. Desroches, A.R. Ingraffea, P.J. Wawrzynek, Simulating fully 3D hydraulic fracturing, in: Modeling in Geomechanics, J. Wiley & Sons, Chichester, 2000, pp. 525–557.
[14] B.A. Schrefler, S. Secchi, L. Simoni, On adaptive refinement techniques in multifield problems including cohesive fracture, Comput. Methods Appl. Mech. Eng. 195 (2006) 444–461.
[15] S. Secchi, L. Simoni, B.A. Schrefler, Mesh adaptation and transfer schemes for discrete fracture propagation in porous materials, Int. J. Numer. Anal. Methods Geomech. 31 (2007) 331–345.
[16] S. Secchi, B.A. Schrefler, A method for 3-D hydraulic fracturing simulation, Int. J. Fract. 178 (2012) 245–258.
[17] L. Simoni, B.A. Schrefler, Multi-field simulation of fracture, Adv. Appl. Mech. 47 (2014) 367–519.
[18] J. Réthoré, R. de Borst, M.A. Abellan, A two-scale approach for fluid flow in fractured porous media, Int. J. Numer. Methods Eng. 75 (2007) 780–800.
[19] J. Réthoré, R. de Borst, M.A. Abellan, A two-scale model for fluid flow in an unsaturated porous medium with cohesive cracks, Comput. Mech. 42 (2008) 227–238.
[20] T. Mohammadnejad, A.R. Khoei, Hydro-mechanical modelling of cohesive crack propagation in multiphase porous media using the extended finite element method, Int. J. Numer. Anal. Methods Geomech. 37 (2013) 1247–1279.
[21] T. Mohammadnejad, A.R. Khoei, An extended finite element method for fluid flow in partially saturated porous media with weak discontinuities: the convergence analysis of local enrichment strategies, Comput. Mech. 51 (2013) 327–345.
[22] J.M. Segura, I. Carol, Coupled HM analysis using zero-thickness interface elements with double nodes. Part I: Theoretical model, Int. J. Numer. Anal. Methods Geomech. 32 (2008) 2083–2101.
[23] J.M. Segura, I. Carol, Coupled HM analysis using zero-thickness interface elements with double nodes. Part II: Verification and application, Int. J. Numer. Anal. Methods Geomech. 32 (2008) 2103–2123.
[24] B. Carrier, S. Granet, Numerical modelling of hydraulic fracture problem in permeable medium using cohesive zone model, Eng. Fract. Mech. 79 (2012) 312–328.
[25] R. de Borst, J. Réthoré, M.A. Abellan, A numerical approach for arbitrary cracks in a fluid-saturated porous medium, Arch. Appl. Mech. 75 (2006) 595–606.
[26] B. Lecampion, An extended finite element method for hydraulic fracture problems, Commun. Numer. Methods Eng. 25 (2009) 121–133.
[27] E. Gordeliy, A. Peirce, Coupling schemes for modeling hydraulic fracture propagation using the XFEM, Comput. Methods Appl. Mech. Eng. 253 (2013) 305–322.
[28] E. Gordeliy, A. Peirce, Enrichment strategies and convergence properties of the XFEM for hydraulic fracture problems, Comput. Methods Appl. Mech. Eng. 283 (2015) 474–502.
[29] E. Gordeliy, A. Peirce, Implicit level set schemes for modeling hydraulic fractures using the XFEM, Comput. Methods Appl. Mech. Eng. 266 (2013) 125–143.
[30] F. Armero, C. Callari, An analysis of strong discontinuities in a saturated poro-plastic solid, Int. J. Numer. Methods Eng. 46 (1999) 1673–1698.
[31] J. Réthoré, R. de Borst, M.A. Abellan, A discrete model for the dynamic propagation of shear bands in a fluid-saturated medium, Int. J. Numer. Anal. Methods Geomech. 31 (2007) 347–370.
[32] J. Larsson, R. Larsson, Localization analysis of a fluid-saturated elastoplastic porous medium using regularized discontinuities, Mech. Cohes. Frict. Mater. 5 (2000) 565–582.
[33] F. Irzal, J.J.C. Remmers, C.V. Verhoosel, R. de Borst, An isogeometric analysis Bézier interface element for mechanical and poromechanical fracture problems, Int. J. Numer. Methods Eng. 97 (2014) 608–628.
[34] J. Vignollet, S. May, R. de Borst, Isogeometric analysis of fluid-saturated porous media including flow in the cracks, Int. J. Numer. Methods Eng. (2016), http://dx.doi.org/10.1002/nme.5242.
[35] F. Irzal, J.J.C. Remmers, J.M. Huyghe, R. de Borst, A large deformation formulation for fluid flow in a progressively fracturing porous material, Comput. Methods Appl. Mech. Eng. 256 (2013) 29–37.
[36] A.R. Khoei, S. Moallemi, E. Haghighat, Thermo-hydro-mechanical modelling of impermeable discontinuity in saturated porous media with X-FEM technique, Eng. Fract. Mech. 96 (2012) 701–723.
[37] R.W. Lewis, B.A. Schrefler, The Finite Element Method in the Static and Dynamic Deformation and Consolidation of Porous Media, 2nd ed., Wiley & Sons, Chichester, 1998.
[38] D.S. Dugdale, Yielding of steel sheets containing slits, J. Mech. Phys. Solids 8 (1960) 100–104.
[39] G.I. Barenblatt, The mathematical theory of equilibrium cracks in brittle fracture, Adv. Appl. Mech. 7 (1962) 55–129.
[40] R. de Borst, Numerical aspects of cohesive zone models, Eng. Fract. Mech. 70 (2003) 1743–1757.
[41] J.R. Rice, D.A. Simons, The stabilization of spreading shear faults by coupled deformation–diffusion effects in fluid-infiltrated porous materials, J. Geophys. Res. 81 (1976) 5322–5334.
[42] R. de Borst, M.A. Crisfield, J.J.C. Remmers, C.V. Verhoosel, Non-Linear Finite Element Analysis of Solids and Structures, 2nd ed., Wiley & Sons, Chichester, 2012.
[43] J.C.J. Schellekens, R. de Borst, On the numerical integration of interface elements, Int. J. Numer. Methods Eng. 36 (1993) 43–66.
[44] E.W. Remij, J.J.C. Remmers, J.M. Huyghe, D.M.J. Smeulders, The enhanced local pressure model for the accurate analysis of fluid driven fracture in porous materials, Comput. Methods Appl. Mech. Eng. 286 (2015) 293–312.
[45] T. Belytschko, T. Black, Elastic crack growth in finite elements with minimal remeshing, Int. J. Numer. Methods Eng. 45 (1999) 601–620.

Please cite this article in press as: R. de Borst, Fluid flow in fractured and fracturing porous media: A unified view, Mech. Re. Commun. (2016), http://dx.doi.org/10.1016/j.mechrescom.2016.05.004

[46] N. Moës, J. Dolbow, T. Belytschko, A finite element method for crack growth without remeshing, Int. J. Numer. Methods Eng. 46 (1999) 131–150.
[47] A. Simone, Partition of unity based discontinuous elements for interface phenomena: computational issues, Commun. Numer. Methods Eng. 20 (2004) 465–478.
[48] I. Babuska, J.M. Melenk, The partition of unity method, Int. J. Numer. Methods Eng. 40 (1997) 727–758.
[49] J.A. Cottrell, T.J.R. Hughes, Y. Bazilevs, Isogeometric Analysis, Wiley & Sons, Chichester, 2009.
[50] C.V. Verhoosel, M.A. Scott, R. de Borst, T.J.R. Hughes, An isogeometric analysis approach to cohesive zone modelling, Int. J. Numer. Methods Eng. 87 (2011) 336–360.
[51] J. Vignollet, S. May, R. de Borst, On the numerical integration of isogeometric interface elements, Int. J. Numer. Methods Eng. 102 (2015) 1733–1749.
[52] F. Irzal, J.J.C. Remmers, C.V. Verhoosel, R. de Borst, Isogeometric finite element analysis of poroelasticity, Int. J. Numer. Anal. Methods Geomech. 37 (2013) 1891–1907.

Please cite this article in press as: R. de Borst, Fluid flow in fractured and fracturing porous media: A unified view, Mech. Re. Commun. (2016), http://dx.doi.org/10.1016/j.mechrescom.2016.05.004